

Nonadditive intermolecular forces from the spectroscopy of van der Waals trimers: A theoretical study of Ar₂-HF

Andreas Ernesti and Jeremy M. Hutson

Department of Chemistry, University of Durham, South Road, Durham, DH1 3LE, England

(Received 19 July 1994)

Calculations of vibrational energies and rotational constants are carried out for the van der Waals trimer Ar₂-HF. The calculations include all five intermolecular degrees of freedom. The different intramolecular vibrational states v of the HF molecule are separated out adiabatically, so that the calculations are carried out on effective intermolecular potentials for each HF vibrational state separately. Calculations are performed both on pairwise-additive potentials, derived from the well-known Ar-Ar and Ar-HF potentials, and on nonadditive potentials, incorporating various different contributions to the three-body forces. The results are compared with experimental results from high-resolution spectroscopy, and provide detailed information on the anisotropy of the nonadditive intermolecular forces. As in previous work on Ar₂-HCl, it is found that a very important nonadditive term arises from the interaction between the permanent multipoles of the HF molecule and the exchange quadrupole caused by distortion of the two Ar atoms as they overlap. An improved model of this term is described.

PACS number(s): 33.20.Vq, 34.20.Gj, 36.40.-c

I. INTRODUCTION

The intermolecular forces between atoms and molecules are of great importance in studies of solids, liquids, and clusters. Over the last decade, enormous advances have been made in our understanding of interaction potentials between atoms and small molecules. In particular, high-resolution spectra of van der Waals complexes have been used to obtain very accurate intermolecular potential energy surfaces for the interaction of Ar atoms with small molecules such as H₂ [1], HF [2], HCl [3], H₂O [4], and NH₃ [5]. In parallel with this work, there have been important developments in *ab initio* techniques for calculating intermolecular potentials.

Despite the advances in our understanding of pair potentials, there remains a major obstacle in using the new potentials for studies of condensed phases. This is the problem of nonadditivity: the total interaction energy of a cluster of molecules is not just the sum of the pairwise interactions, but also includes three-body and higher n -body terms [6]. For the rare gas solids, for example, nonadditive terms are known to contribute up to 10% to the binding energy. Unfortunately, most of the work so far on nonadditive forces has been for purely atomic systems; for systems containing molecules, there are no reliable models of the nonadditive forces. This effectively precludes the use of accurate pair potentials in simulations of condensed phases.

There are many properties of matter that depend on nonadditive interactions, but it is difficult to find experiments that contain sufficiently detailed information to allow information on the three-body forces to be extracted. The first prerequisite is that the pair potentials involved should be known very accurately, so that the

effects of nonadditive forces can be isolated. Until recently, sufficiently accurate pair potentials were available only for the rare gas pairs. However, as described above, very good pair potentials are now available for simple molecular systems such as Ar-HF and Ar-HCl. In addition, it has recently become possible to measure high-resolution microwave, far-infrared, and infrared spectra of van der Waals trimers such as Ar₂-HCl [7-10] and Ar₂-HF [11,12]. The trimer spectra are very sensitive to details of the interaction potential, so that there is now the possibility of obtaining definitive experimental information on nonadditive forces in systems containing molecules.

Some progress has already been made toward this objective. Hutson *et al.* [13] carried out restricted dimensionality calculations on Ar₂-HCl, and established that the microwave spectra [7] contained valuable information on three-body forces. They also pointed out that far-infrared spectra would sample the nonadditive forces over a much wider range of geometries, and might allow the *determination* of the three-body forces. This stimulated extensive experimental work on the far-infrared spectroscopy of Ar₂-HCl [8-10]. Cooper and Hutson [14] developed a computational method for calculating the vibration-rotation energy levels of complexes such as Ar₂-HX ($X=F, Cl, Br, \text{etc.}$), including all five low-frequency degrees of freedom. They showed that the frequencies of the intermolecular bending bands in the far-infrared spectrum of Ar₂-HCl are very sensitive to three-body forces, and that there are significant discrepancies between the predictions of pairwise-additive potentials and the experimental results. In addition, they showed that "conventional" types of nonadditive interaction, such as the Axilrod-Teller triple-dipole term and the interactions between the induced dipoles on the two Ar atoms, were

not sufficient to resolve the discrepancies.

Cooper and Hutson identified a new type of non-additive force that is expected to be important in all molecular systems. This arises when two atoms or molecules come close together and distort, so that their multipole moments are modified: if the third body in the system is a molecule (rather than an atom), the distortion modifies the electrostatic interaction, and can thus have a large effect on the energy. For $\text{Ar}_2\text{-HCl}$, the important interaction is that between the distorted charge distributions of the Ar atoms and the permanent multipole moments of the HCl molecule. In Ref. [14], the charge distribution of the distorted Ar_2 moiety was represented by a quadrupole moment at the Ar_2 midpoint, which was then allowed to interact with the dipole and quadrupole moments of HCl; this was termed the “exchange quadrupole” interaction. Including the exchange quadrupole term was found to give a good qualitative explanation of the experimental results.

This model has also been applied to the far-infrared spectrum of $\text{Ar}_2\text{-DCl}$ [15] and to the vibrational shifts in the infrared fundamental band of $\text{Ar}_2\text{-HF}$ [16]. In all these cases, the exchange quadrupole interaction was found to be the only term large enough to explain the discrepancies between the pairwise-additive calculations and the experimental data. However, the model used for this term in Refs. [14–16] overestimates the correction required: a rather smaller three-body term is actually needed to give agreement between experiment and theory. Very recently, Farrell and Nesbitt [17] have succeeded in measuring spectra of $\text{Ar}_2\text{-HF}$ that correspond to excitation of intermolecular bending bands involving hindered internal rotation of HF in combination with the HF stretch. In preliminary calculations on these bands, we have found that our previous model overestimates the corrections needed even more drastically than for $\text{Ar}_2\text{-HCl}$. It is thus clear that an improved model of the exchange multipole forces is needed. In addition, a model designed to interpret the infrared combination bands must include the dependence of the additive and nonadditive forces on the HF stretching state. The purpose of the present paper is to describe such a model, and to apply it to the bending bands of $\text{Ar}_2\text{-HF}$.

There have also been some *ab initio* studies of nonadditive forces in $\text{Ar}_2\text{-HX}$ systems [18,19]. *Szczyński et al.* [19] carried out calculations on $\text{Ar}_2\text{-HCl}$ and $\text{Ar}_2\text{-HF}$ using supermolecular Møller-Plesset perturbation theory calculations, and decomposed the resulting energies into contributions from different physical effects. Unfortunately, they confined their attention to geometries with the HX molecule in the heavy-atom plane, so that it is not possible to use their results directly in dynamical calculations.

The structure of the present paper is as follows. Section II will describe the pairwise-additive potentials used for Ar-Ar and Ar-HF, and the various nonadditive terms considered. Sections III and IV will describe the computational method used for calculating the energy levels and other spectroscopic quantities. Section V will describe the results of the calculations, and Sec. VI will summarize our conclusions.

II. COORDINATE SYSTEM AND POTENTIAL ENERGY SURFACES

The coordinate system used for $\text{Ar}_2\text{-HF}$ is shown in Fig. 1. The positions of the two Ar atoms and the HF center of mass are described by a set of Jacobi coordinates: the Ar-Ar distance is denoted ρ , the distance from the HF center of mass to the Ar_2 center of mass is denoted R , and the angle between the vectors corresponding to R and ρ is denoted χ . The HF bond length is denoted r , and the angle between the r and R vectors is θ , with $\theta = 0^\circ$ corresponding to the H atom of HF pointing directly towards the Ar_2 center of mass. Finally, the angle ϕ is the torsional angle between the r and ρ axes, viewed along R : $\phi = 0^\circ$ corresponds to HF lying in the plane of the heavy atoms, while $\phi = 90^\circ$ is the out-of-plane geometry.

$\text{Ar}_2\text{-HF}$ is a highly asymmetric top: the c axis is perpendicular to the plane of the heavy atoms, and the b axis lies close to R .

A. Pairwise-additive potentials

The pair potentials used in the present work follow.

(1) The Ar-Ar Hartree-Fock dispersion individually damped (HFDID1) potential of Aziz [20]. This potential is the most recent fit to a wide range of experimental data, including both bulk properties such as second virial coefficients and transport coefficients and microscopic properties such as molecular beam scattering results and vibration-rotation energy levels. The potential gives highly accurate vibrational frequencies and rotational constants for the Ar dimer.

(2) The Ar-HF H6(4,3,2) potential of Hutson [2]. This potential energy surface was fitted to spectroscopic constants obtained from 24 different bands in the microwave, far-infrared, and mid-infrared spectra of Ar-HF ($v = 0, 1$ and 2) and Ar-DF ($v = 0$ and 1). The potential includes both the anisotropy and the dependence on the vibrational state v of the HF molecule; the latter is built in parametrically, in terms of the mass-reduced vibrational quantum number

$$\eta = (v + \frac{1}{2})/\mu_{\text{HF}}^{1/2}, \quad (1)$$

where μ_{HF} is the reduced mass of the HF molecule.

These two potentials are used to build up v -dependent pairwise-additive potential energy surfaces for $\text{Ar}_2\text{-HF}$.

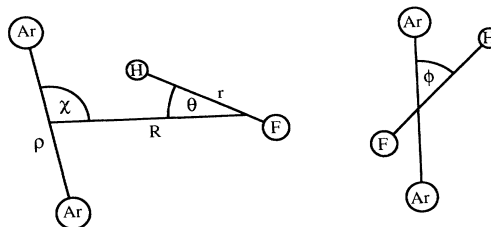


FIG. 1. Coordinate system used for $\text{Ar}_2\text{-HF}$.

Contour plots of various cuts through the additive surfaces are shown in Fig. 2. The heavy atoms form an obtuse isosceles triangle at the equilibrium geometry, with $\chi = 90^\circ$ and the H atom of HF pointing to the center of mass of the Ar dimer, $\theta = 0^\circ$. The HF molecule executes very wide-amplitude bending motions in the angles θ and ϕ , sampling angles up to $\theta = 80^\circ$ even in the ground state. The bending motion of the Ar-Ar fragment, represented by the angle χ , is much more hindered: values of χ between about 75° and 105° are sampled in the ground state. The amplitudes of motion in the R and ρ coordinates are both about $\pm 0.5 \text{ \AA}$.

In comparing calculated quantities with experimental results for the HF bending bands in $\text{Ar}_2\text{-HF}$, the qual-

ity of the Ar-HF pair potential is crucial. The H6(4,3,2) potential has proved to be remarkably successful in predicting the results of experiments that were not included in determining it. A variety of new bands in the infrared spectrum of Ar-HF have been predicted to within 0.1 cm^{-1} [21,22]. In addition, the potential has been used successfully to model state-to-state inelastic differential cross sections [23] and the widths and shifts of pressure-broadened infrared spectra of HF in Ar [24,25]. We estimate that the remaining uncertainties in the Ar-HF pair potential lead to uncertainties of $\pm 0.3 \text{ cm}^{-1}$ in the frequencies of HF bending bands in $\text{Ar}_2\text{-HF}$. The uncertainties due to the Ar-Ar potential are even smaller than this. The computational method and basis sets used in the

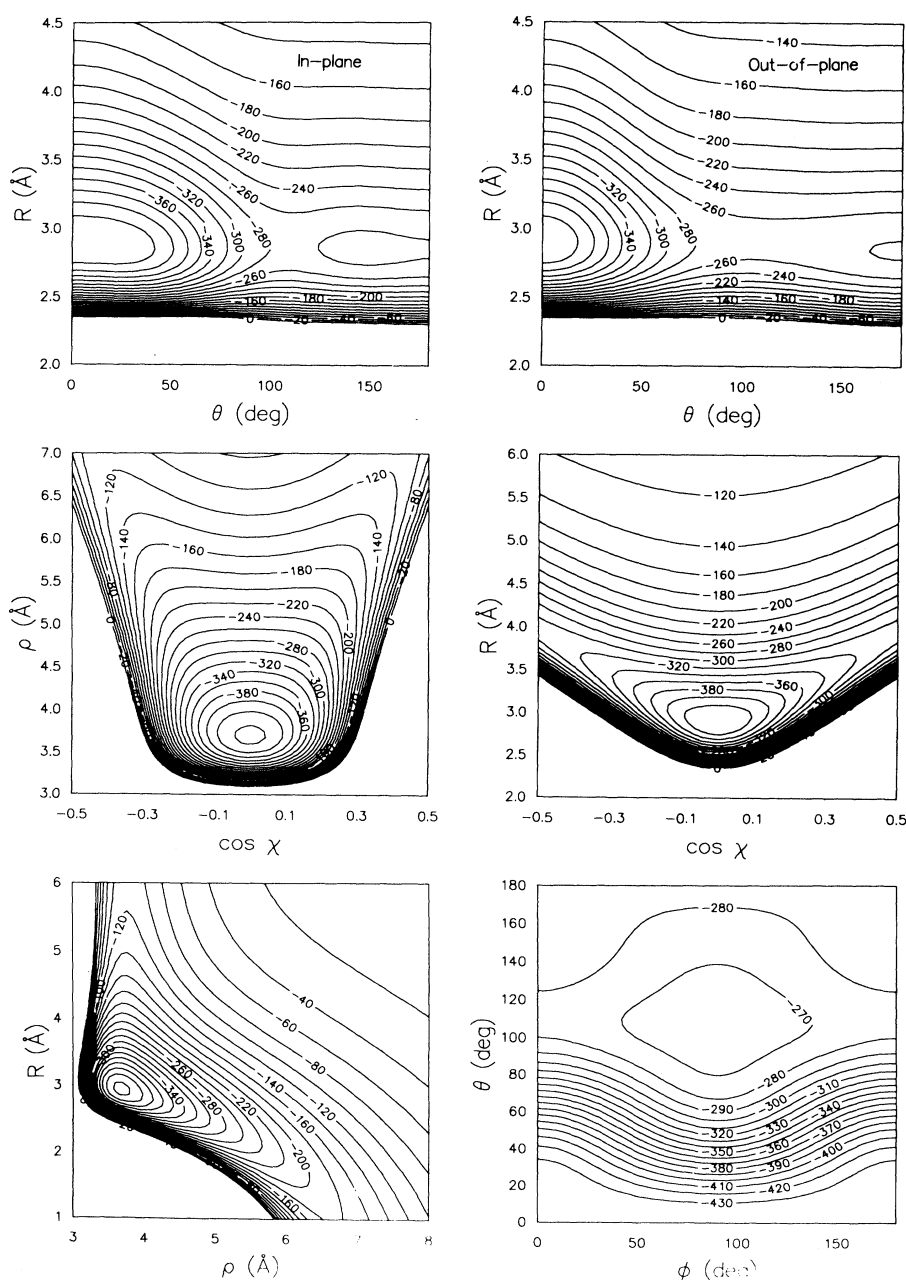


FIG. 2. Contour plots of cuts through the pairwise-additive H6(4,3,2) + HFDID1 potential for $v = 1$. For each contour plot, the coordinates that were not varied were fixed at the values $R = 2.89 \text{ \AA}$, $\rho = 3.82 \text{ \AA}$, $\chi = 90^\circ$, with $\phi = 0^\circ$ for in-plane geometries and $\phi = 90^\circ$ for out-of-plane geometries. Contours are labeled in cm^{-1} .

present work lead to uncertainties of about $\pm 0.2 \text{ cm}^{-1}$. Thus, in general terms, we consider that any discrepancies greater than $\pm 0.5 \text{ cm}^{-1}$ between the experimental results and calculations on pairwise-additive potentials may be attributed to nonadditive intermolecular forces.

B. Nonadditive forces

1. Dispersion contributions

In atomic systems, the most important nonadditive forces are those arising from dispersion. The leading term in the three-body dispersion interaction is the well-known Axilrod-Teller triple-dipole term [26], which for atomic systems takes the form

$$V_{ddd} = 3Z_{ddd}^{(3)} \left(\frac{3 \cos \theta_1 \cos \theta_2 \cos \theta_3 + 1}{r_1^3 r_2^3 r_3^3} \right), \quad (2)$$

where r_1 , r_2 , and r_3 are the lengths of the sides of the triangle formed by the three atoms and θ_1 , θ_2 , and θ_3 are the corresponding internal angles of the triangle. The coefficient $\nu_{123} = 3Z_{ddd}^{(3)} = 269.9 E_h a_0^9$ for $\text{Ar}_2\text{-HF}$ has been evaluated by Kumar and Meath [27] from the dipole oscillator strength distributions of Ar and HF. However, this value is appropriate for $r = r_e$ (corresponding to a mass-reduced quantum number $\eta = 0$), and we require a coefficient that includes the dependence on η . In the present work, we have assumed that the Axilrod-Teller coefficient has the same η dependence as the Ar-HF C_6 coefficient of Ref. [2], so that

$$\nu_{123}(\eta) = \nu_{123}(0)[1 + 0.0239\eta/u^{-1/2}], \quad (3)$$

where u is the unified atomic mass unit.

In molecular systems, the triple-dipole interaction is much more complicated because of the anisotropy of molecular polarizabilities. An approximate form for the triple-dipole energy under these circumstances has been given by Stogryn [28],

$$V_{DDD} = \frac{\nu_{123}}{3\bar{\alpha}_1\bar{\alpha}_2\bar{\alpha}_3} (T_{12})_{\alpha\beta} (T_{23})_{\gamma\delta} (T_{31})_{\mu\nu} \times (\alpha_1)_{\nu\alpha} (\alpha_2)_{\beta\gamma} (\alpha_3)_{\delta\mu}, \quad (4)$$

where α_i is the polarizability tensor and $\bar{\alpha}_i$ is the mean polarizability for particle i . T_{ij} is a symmetric orientation tensor, with Cartesian components

$$(T_{ij})_{\alpha\beta} = \frac{3(\hat{\mathbf{r}}_{ij})_{\alpha}(\hat{\mathbf{r}}_{ij})_{\beta} - \delta_{\alpha\beta}}{|r_{ij}|^3}, \quad (5)$$

and $(\hat{\mathbf{r}}_{ij})_{\alpha}$ is the component of the unit vector between particles i and j along Cartesian axis α . Equation (4) uses the usual summation convention, summing over all repeated suffixes representing Cartesian axes.

In the present work, V_{DDD} was evaluated using $\alpha_{\text{Ar}} = 11.096 a_0^3$ [29] and the η -dependent HF polarizabilities $\alpha_{\parallel}(\eta)$ and $\alpha_{\perp}(\eta)$ of Ref. [2]. A contour plot of the resulting contribution in the (R, θ) plane is shown in Fig. 3; it

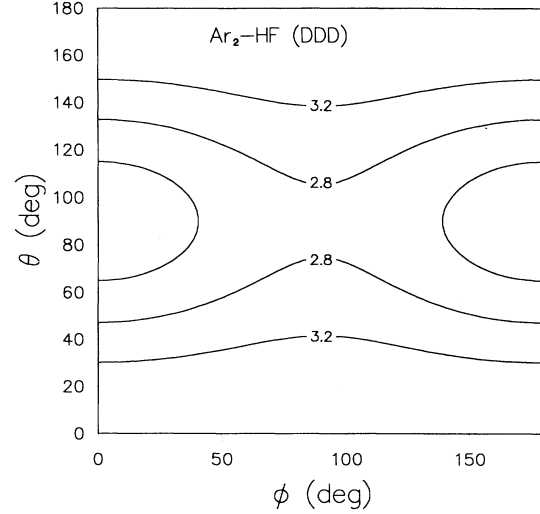


FIG. 3. Contour plot of the dispersion contribution V_{DDD} to the intermolecular potential for $\text{Ar}_2\text{-HF}$ ($v = 1$), for $R = 2.89 \text{ \AA}$, $\rho = 3.82 \text{ \AA}$, and $\chi = 90^\circ$.

is repulsive for all angles around the equilateral geometry. However, it depends only weakly on the HF orientation, and so may be expected to have relatively little effect on the HF bending frequencies in the trimer.

For pair potentials, it is well known that the dispersion interaction must be damped when overlap is significant, to prevent the inverse power terms dominating the potential at short range. In principal, analogous damping functions are needed for nonadditive dispersion terms [30,31]. However, damping functions for three-body interactions are not as well understood as for pair potentials, and it has been shown for $\text{Ar}_2\text{-HCl}$ [14] that damping the triple-dipole term has little effect on the bending energy levels. Accordingly, the triple-dipole formula was used without damping in the present work.

2. Induction contributions

In a complex such as $\text{Ar}_2\text{-HF}$, the highly polar HF molecule creates substantial electric fields at the locations of the two Ar atoms. These fields (and the corresponding field gradients) polarize the Ar atoms, producing induced dipole moments (and higher multipoles). The interactions between the induced moments and the permanent moments of the HF are already taken into account in the Ar-HF pair potential, but there is a nonadditive energy contribution arising from the interactions between the induced moments on the two Ar atoms.

The electrostatic potential V at atom i is

$$V = \sum_l Q_l P_l(\cos \vartheta_i) / R_i^{l+1}, \quad (6)$$

where Q_l is the 2^l -pole moment of HX, $P_l(x)$ is a Legendre polynomial, and $R_i, \vartheta_i, \varphi_i$ are the coordinates of

atom i in an axis system with its z axis along the XH bond. The corresponding components of the electric field are

$$\begin{aligned} F_x &= \sum_l [Q_l P'_{l+1}(\cos \vartheta_i) \sin \vartheta_i \cos \varphi_i] / R_i^{l+2}, \\ F_y &= \sum_l [Q_l P'_{l+1}(\cos \vartheta_i) \sin \vartheta_i \sin \varphi_i] / R_i^{l+2}, \\ F_z &= \sum_l (l+1) Q_l P'_{l+1}(\cos \vartheta_i) / R_i^{l+2}, \end{aligned} \quad (7)$$

where $P'_l(x) = dP_l(x)/dx$. If only the dipole polarizability of the Ar atoms is included, the fields produce induced dipoles with Cartesian components $\mu_\beta^{\text{ind}} = \alpha_{\text{Ar}} F_\beta$.

In previous work, the fields at the two Ar atoms were evaluated, including HX multipole moments up to hexadecapole, and the interaction energy of the two induced dipoles was calculated from

$$V_{\text{ind}} = -[3(\mu_1^{\text{ind}} \cdot \hat{\rho})(\mu_2^{\text{ind}} \cdot \hat{\rho}) - \mu_1^{\text{ind}} \cdot \mu_2^{\text{ind}}] / \rho^3, \quad (8)$$

where $\hat{\rho}$ is a unit vector along the Ar-Ar axis. The energy contribution resulting from this treatment for $\text{Ar}_2\text{-HF}$ is shown in the center right panel of Fig. 4. However, as will be seen below, there are important cross terms between the induced dipoles and other effects. We will therefore postpone further consideration of the induction forces to the next subsection.

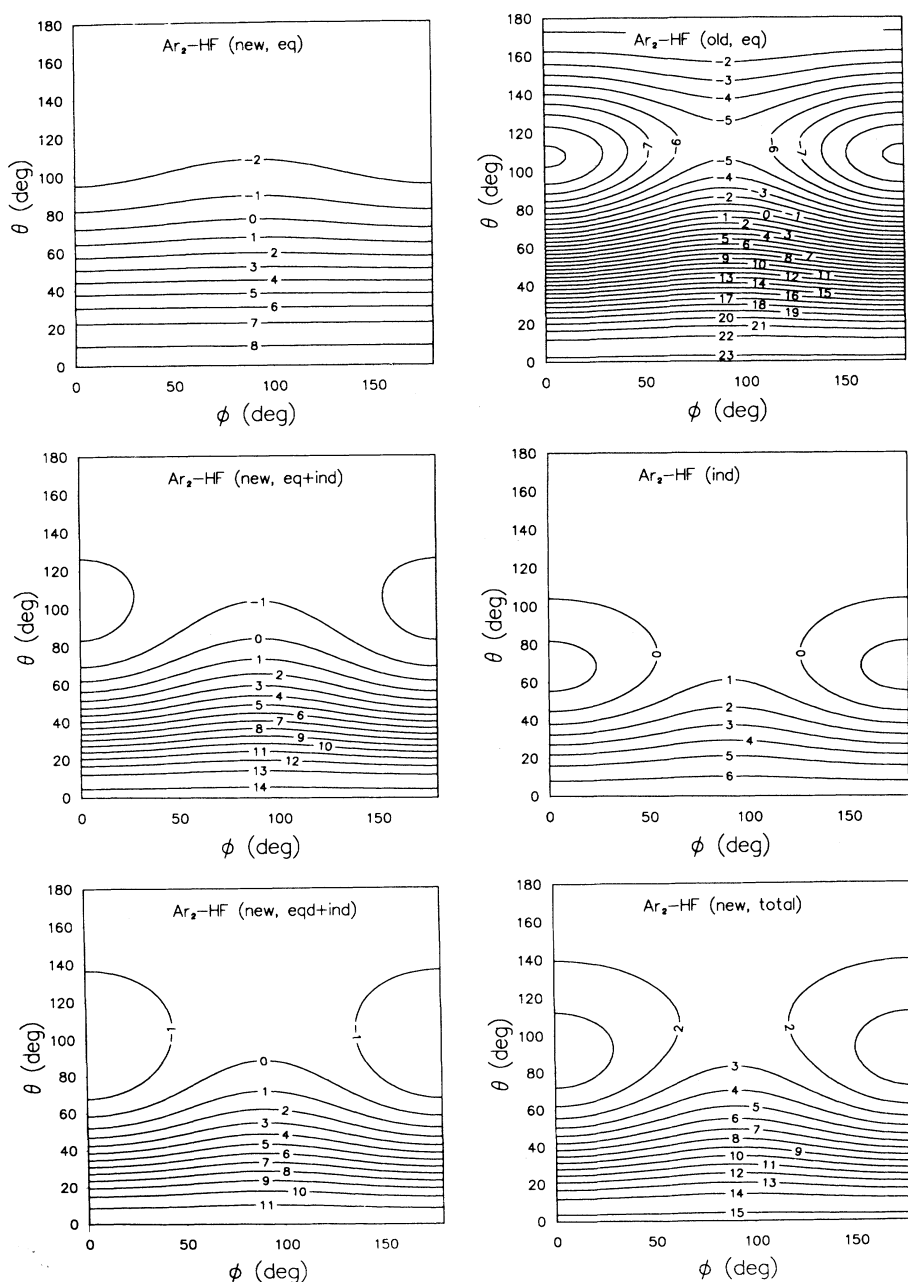


FIG. 4. Contour plots of various nonadditive contributions to the intermolecular potential for $\text{Ar}_2\text{-HF}$ ($v = 1$). All cuts through the potential are for $R = 2.89 \text{ \AA}$, $\rho = 3.82 \text{ \AA}$, and $\chi = 90^\circ$. The panel labels indicate (old, eq): exchange quadrupole contribution, modeled by a central quadrupole at the Ar_2 midpoint; (new, eq): exchange quadrupole contribution, modeled by two dipoles at the Ar atoms; (new, eq+ind): contribution from the new model of the exchange interaction and the induction term, including cross terms; (ind): induction contribution alone; (new, eqd+ind): as (new, eq+ind) but including the dispersion contribution to the Ar_2 quadrupole; (new, total): sum of all contributions discussed, including the triple-dipole term.

3. *Overlap-dependent contributions*

In previous work, we considered short-range non-additive forces arising from two different sources.

First, there is a short-range term analogous to that for Ar₃, termed the exchange overlap contribution [32]: when two atoms or molecules approach one another closely, their electron clouds distort away from one another in such a way as to reduce overlap. This distortion modifies their overlap with a third body; if the third body is near the axis of the first two, the overlap is increased and there is a positive contribution to the three-body energy. Conversely, for near-equilateral geometries, the deformation produces a negative contribution to the three-body energy. The previous work on Ar₂-HCl [14] showed that the exchange overlap term makes very small contributions to the nonadditive shifts; accordingly, it has not been included in the present study.

Secondly, as described in the Introduction, the overlap distortion of the two Ar atoms produces a quadrupole moment on the Ar₂ pair, and this can interact with the permanent multipoles of the HF molecule. This gives rise to an important electrostatic contribution to the non-additive forces. In our previous work, this interaction was calculated by representing the distorted charge distribution of the two Ar atoms by a ρ -dependent point quadrupole $\Theta(\rho)$ located at the midpoint of Ar₂. However, the midpoint is usually considerably closer to HF than either of the Ar atoms, and this model substantially overestimates the field that results at the HF molecule. It is much better to use a distributed multipole representation of the Ar₂ charge distribution. The simplest possible distributed representation, which is used in the present work, is to replace the Ar₂ quadrupole with two equal and opposite dipoles μ_i^{eqd} located on the Ar atoms,

$$\mu_1^{\text{eqd}} = -\mu_2^{\text{eqd}} = \frac{1}{2}\Theta(\rho)\hat{\rho}/\rho, \quad (9)$$

where the superscript eqd indicates exchange quadrupole plus dispersion. The quadrupole moment $\Theta(\rho)$ of the Ar₂ pair is evaluated using the functional form

$$\Theta(\rho) = -\frac{1}{2}e\rho^2 \frac{\exp(-\frac{1}{2}\beta_{\text{eq}}^2\rho^2)}{1 - \exp(-\frac{1}{2}\beta_{\text{eq}}^2\rho^2)} + \Theta_6/\rho^6. \quad (10)$$

The first term in Eq. (10) is termed the exchange quadrupole (eq) contribution, and is represented here using a functional form derived by Jansen [33] from a single-electron approximation. However, Jansen's value of β_{eq} is known to produce a substantial overestimate of the exchange quadrupole, so we used instead a value $\beta_{\text{eq}} = 0.936 \text{ \AA}^{-1}$, obtained by fitting to self-consistent-field (SCF) calculations of the short-range overlap quadrupole of Ar₂ [34]. The second term in Eq. (10) arises from dispersion [35], and was not included in our earlier work on Ar₂-HX, but in fact can make a significant contribution: in the present work, the quadrupole dispersion coefficient Θ_6 is estimated as $\Theta_6 = (\frac{5}{2}B_{\text{Ar}}/\alpha_{\text{Ar}})C_6$ [36], where B_{Ar} is the quadrupole hyperpolarizability of the Ar atom and C_6 is the (negative) dispersion energy coefficient for Ar-Ar. The value used in the present work, $\Theta_6 = 2086 e a_0^8$,

is based on the C_6 coefficient for the HFDID1 potential [20] and the ratio of B_{Ar} and α_{Ar} obtained from SCF calculations by Maroulis and Bishop [37]. The dispersion contribution to $\Theta(\rho)$ is of opposite sign to the exchange quadrupole term, and about 30% as large at the equilibrium geometry.

It is straightforward to calculate the energy contributions arising from interaction of either the central quadrupole or the distributed dipoles with the permanent multipoles of HF using standard electrostatic formulas [38]. In the present work, the HF charge distribution was represented by a single-center multipole expansion, including multipoles up to the hexadecapole at the HF center of mass. The results of the central quadrupole (old) and distributed dipole (new) representations, neglecting the dispersion term involving Θ_6 , are compared in the top panels of Fig. 4. It may be seen that the two results are substantially different: the distributed dipole representation gives a much smaller energy contribution, though the term is still substantially larger and more anisotropic than the triple-dipole term, V_{DDD} . The distributed dipole representation actually somewhat underestimates the field at the HF center of mass for the equilibrium geometry, and thus underestimates the interaction energy. It would clearly be desirable to use a more sophisticated distributed representation of the Ar₂ charge distribution, but not enough is known about the ρ dependence to allow this at present.

In previous work, the exchange quadrupole term and the induction term were evaluated independently. However, the present treatment makes it clear that both effects produce dipole moments (and, in principle, higher moments) on the Ar atoms. There are thus cross terms involving interactions between the dipole moments arising from the two sources. In the present work, therefore, we calculate the vector sum of the two dipole contributions on each atom, $\mu_i^{\text{tot}} = \mu_i^{\text{ind}} + \mu_i^{\text{eqd}}$. The energies of interaction between the two total dipoles and between each of them and the multipole moments on the HX molecule are easily calculated. However, care is needed to avoid double counting: all contributions that are part of the Ar-Ar and Ar-HX pair potentials must be excluded from the three-body terms. The interactions between μ_i^{ind} and the HX multipoles and between μ_1^{eqd} and μ_2^{eqd} are of this type. The resulting three-body term is thus

$$\begin{aligned} V_3 = & -\mathbf{F}_1 \cdot \mu_1^{\text{eqd}} - \mathbf{F}_2 \cdot \mu_2^{\text{eqd}} \\ & - [3(\mu_1^{\text{tot}} \cdot \hat{\rho})(\mu_2^{\text{tot}} \cdot \hat{\rho}) - \mu_1^{\text{tot}} \cdot \mu_2^{\text{tot}}]/\rho^3 \\ & + [3(\mu_1^{\text{eqd}} \cdot \hat{\rho})(\mu_2^{\text{eqd}} \cdot \hat{\rho}) - \mu_1^{\text{eqd}} \cdot \mu_2^{\text{eqd}}]/\rho^3. \end{aligned} \quad (11)$$

Since μ_1^{eqd} and μ_2^{eqd} are directed along $\hat{\rho}$, and are equal and opposite, the last term simplifies to $-2|\mu_1^{\text{eqd}}|^2/\rho^3 = -\frac{1}{2}[\Theta(\rho)]^2/\rho^5$.

The energy contributions resulting from this treatment are shown in the two lower left panels of Fig. 4, with and without the dispersion quadrupole. It may be noted that, in Ar₂-HF, the exchange quadrupole (eq) and induction (ind) terms are of comparable magnitude. However, it should be emphasized that, in the present model, the "eq+ind" result is not just the sum of the "eq" and "ind"

terms, but also includes cross terms.

The dependence of the nonadditive terms on the HF vibrational level v is easily built in by using v -dependent (or η -dependent) values of the HF multipole moments Q_l . In the present work, the HF dipole and quadrupole were represented using the η dependent functions given in Table I of Ref. [2], and the HF octopole and hexadecapole were taken from the work of Bulanin *et al.* [39]; the η dependence of the octopole and hexadecapole was neglected.

III. COMPUTATIONAL METHOD

The computational method used in the present work is discussed in detail in Ref. [14], and will be described only briefly here.

The vibrational Hamiltonian for the Ar₂-HF trimer, neglecting some kinetic energy terms involving mixed derivatives between θ and χ , is

$$\begin{aligned} \hat{H}_{\text{vib}} = & -\frac{\hbar^2}{2\mu R} \left(\frac{\partial^2}{\partial R^2} \right) R - \frac{\hbar^2}{M_{\text{Ar}}\rho} \left(\frac{\partial^2}{\partial \rho^2} \right) \rho \\ & + \left(\frac{\hbar^2}{2\mu R^2} + \frac{\hbar^2}{M_{\text{Ar}}\rho^2} \right) \frac{\partial}{\partial \cos \chi} \left[\sin^2 \chi \frac{\partial}{\partial \cos \chi} \right] \\ & + \left(b_v + \frac{\hbar^2}{2\mu R^2} \right) \hat{j}_{\text{HF}}^2 + V_v(R, \rho, \chi, \theta, \phi), \quad (12) \end{aligned}$$

where $\mu = 2M_{\text{Ar}}M_{\text{HF}}/(2M_{\text{Ar}} + M_{\text{HF}})$ is the reduced mass of the diatom-diatom complex, \hat{j}_{HF} is the body-fixed angular momentum operator for the rotation of HF in the trimer, and b_v is the rotational constant of the HF molecule for the vibrational state concerned. The Hamiltonian depends on the complete intermolecular potential $V_v(R, \rho, \chi, \theta, \phi)$, which is averaged over the vibrational motion of HF in the adiabatically decoupled vibrational state v . The five-dimensional vibrational problem for the Ar₂-HF complex is solved for each such state v by diagonalizing a single Hamiltonian matrix using a non-orthogonal basis set:

(1) For the R coordinate, a distributed Gaussian basis set [40] is used, with N_i Gaussian functions $\psi_i(R)$ distributed on an equally spaced grid between the limits R_{min} and R_{max} . The basis set used here had $N_i = 16$ Gaussians, with $R_{\text{min}} = 2.5 \text{ \AA}$ and $R_{\text{max}} = 5.0 \text{ \AA}$.

(2) For the ρ and χ coordinates, orthonormal sets of suitably adapted one-dimensional basis functions, $\Upsilon_w(\rho)$ and $\Phi_u(\cos \chi)$, are used. These functions are defined as eigenfunctions of effective potentials for the ρ and χ motions, as described below. The resulting product basis set is restricted by the conditions $w \leq w_{\text{max}}$ and $w + u \leq q_{\text{max}}$; in the present work, we used $w_{\text{max}} = 2$ and $q_{\text{max}} = 4$.

(3) For the angular motion of the HF molecule, a basis set of spherical harmonics $Y_{jk}(\theta, \phi)$ with $j_{\text{max}} = 5$ is used, excluding the functions with $j = 4$, $k = 4$ and $j = 5$, $k > 1$.

The vibrational basis functions may be classified according to their symmetry (+ or -) under exchange of the two argon atoms, (12), and the inversion operation,

E^* . The resulting symmetry labels η and ϵ are 0 or 1, indicating the symmetries $(-1)^\eta$ and $(-1)^\epsilon$ under (12) and E^* , respectively (see also Ref. [14]). The symmetrized basis functions are given by

$$\begin{aligned} \Psi_{i w u j k}^{\eta \epsilon}(R, \rho, \chi, \theta, \phi) = & [2(1 + \delta_{k0})]^{-1/2} \\ & \times \Psi_i(R) \Upsilon_w(\rho) \Phi_u(\cos \chi) \\ & \times [Y_{jk}(\theta, \phi) + (-1)^{k+\epsilon} Y_{j-k}(\theta, \phi)], \quad (13) \end{aligned}$$

where δ_{k0} is the Kronecker symbol. Because of the symmetry, $u + k$ and η must be either both even or both odd. The Hamiltonian matrix thus factorizes into four independent blocks.

The basis functions $\Upsilon_w(\rho)$ and $\Phi_u(\cos \chi)$ are defined to be eigenfunctions of one-dimensional Hamiltonian operators.

(1) For the coordinate ρ , the Hamiltonian defining the basis set is

$$\hat{H}_\rho = -\frac{\hbar^2}{M_{\text{Ar}}\rho} \left(\frac{\partial^2}{\partial \rho^2} \right) \rho + V_{\text{eff}}(\rho). \quad (14)$$

This contains a one-dimensional effective potential $V_{\text{eff}}(\rho)$. The convergence of the five-dimensional calculation naturally depends on the choice of this potential. For Ar₂-HF, we have found that basis functions derived using an adiabatic potential $V_{\text{eff}}(\rho)$ as described by Elrod *et al.* [15] give slightly better convergence than those obtained using a simple cut through the complete potential as used in Ref. [14]. In the present work, therefore, we follow Ref. [15]: for each value of ρ , a three-dimensional problem in R , θ , and ϕ is solved, with χ fixed at 90° . This defines a set of adiabatic potentials $U_m(\rho)$. The Ar-Ar stretching basis functions $\Upsilon_w(\rho)$ are taken to be eigenfunctions of the Hamiltonian (14) with $V_{\text{eff}}(\rho) = U_0(\rho)$.

(2) For the coordinate χ , the Hamiltonian defining the basis set is

$$\begin{aligned} \hat{H}_\chi = & \left(\frac{\hbar^2}{2\mu R_{\text{cut}}^2} + \frac{\hbar^2}{M_{\text{Ar}}\rho_{\text{cut}}^2} \right) \\ & \times \frac{\partial}{\partial \cos \chi} \left[\sin^2 \chi \frac{\partial}{\partial \cos \chi} \right] + V_{\text{eff}}(\cos \chi). \quad (15) \end{aligned}$$

In this case, the effective potential $V_{\text{eff}}(\cos \chi)$ is taken to be a cut through the full potential, $V(R_{\text{cut}}, \rho_{\text{cut}}, \chi, \theta = 0^\circ, \phi = 0^\circ)$. To choose R_{cut} , a three-dimensional problem in R , θ , and ϕ is solved; ρ and χ are clamped at their equilibrium values, and R_{cut} is taken to be $\langle R \rangle_1$, the expectation value of R for the first excited stretching state. The value of ρ_{cut} is chosen to be $\langle \rho \rangle_1$, the expectation value of ρ for the basis function $\Upsilon_1(\rho)$.

The full Hamiltonian matrix is constructed in the non-orthogonal basis set (13), as described in Ref. [14]. The resulting generalized eigenvalue problem is then solved using routines from the NAG FORTRAN Library [41]. The resulting wave functions are given by

$$\Psi_n^{\eta \epsilon} = \sum_{i w u j k} c_{n i w u j k}^{\eta \epsilon} \Psi_{i w u j k}^{\eta \epsilon}. \quad (16)$$

The wave functions are used to calculate rotational constants as described below, and overall band intensities as described in Ref. [14].

IV. ROTATIONAL STRUCTURE

It is not at present feasible to solve the full vibration-rotation problem for total angular momentum $J > 0$. Because of this, rotational constants must be calculated from expectation values involving the vibrational wave functions. In previous work on van der Waals trimers [13–15], rotational constants were calculated from expectation values based on formulas that assumed that one of the inertial axes always lies along the intermolecular vector R . However, we have recently shown that, for complexes containing fragments with large moments of inertia, this approximation can lead to errors of several percent [42]. More accurate expressions can be obtained by applying the Eckart conditions explicitly to obtain inertial axes that move as the molecule vibrates. In Ref. [42], we described how to apply this procedure in Jacobi coordinates for a complex formed from an atom and a linear molecule. If the HF molecule is approximated as a point mass, the formulas of Ref. [42] can be applied to Ar₂-HF. For a triatomic complex with a C_{2v} equilibrium geometry described by coordinates R_0 and ρ_0 , the angle α between the R vector and the nearby inertial axis (b in the present case) is

$$\tan \alpha = \frac{\delta \cos \chi}{1 + \delta \sin \chi}, \quad (17)$$

where $\delta = \mu_{\text{Ar}_2} \rho_0 / \mu R R_0$ and $\mu_{\text{Ar}_2} = M_{\text{Ar}}/2$. Inverting the moment of inertia tensor, the rotational constants can be shown to be [42]

$$A = \frac{\hbar^2}{2} \left\langle \frac{\mu R^2 \sin^2 \alpha + \mu_{\text{Ar}_2} \rho^2 \sin^2 \beta}{\mu R^2 \mu_{\text{Ar}_2} \rho^2 \sin^2 \chi} \right\rangle, \quad (18a)$$

$$B = \frac{\hbar^2}{2} \left\langle \frac{\mu R^2 \cos^2 \alpha + \mu_{\text{Ar}_2} \rho^2 \cos^2 \beta}{\mu R^2 \mu_{\text{Ar}_2} \rho^2 \sin^2 \chi} \right\rangle, \quad (18b)$$

$$C = \frac{\hbar^2}{2} \left\langle \frac{1}{\mu R^2 + \mu_{\text{Ar}_2} \rho^2} \right\rangle, \quad (18c)$$

where $\beta = \chi + \alpha$. These expressions are more accurate than those used in Refs. [14,15] for Ar₂-HCl and Ar₂-DCl, but nevertheless neglect the structure of the HX molecule, treating it as a point particle. This approximation is likely to cause the rotational constants to be overestimated by a few MHz. However, a more serious approximation is that the expressions above also neglect Coriolis coupling. For triatomic complexes, Coriolis coupling affects only the out-of-plane rotational constant [42], but the effects are not as simple in the present case.

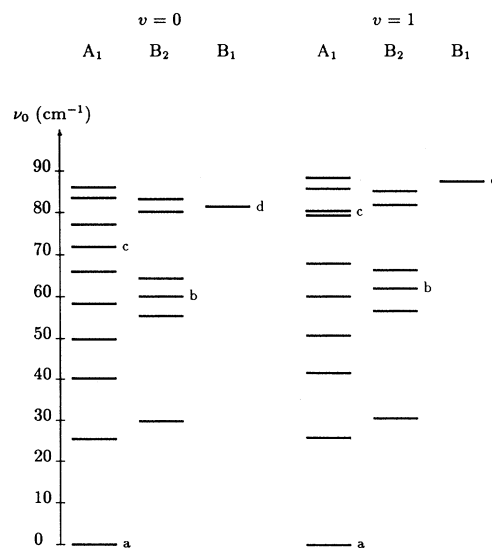
In the present calculation, the expectation values of the rotational constants were evaluated by numerical quadrature over R , ρ , and χ . The integrals over ρ and χ were carried out by Gauss-Hermite quadrature, and those over R by the trapezium rule. Since the operators in (18) do not depend on θ and ϕ , and the spherical harmonics

$Y_{jk}(\theta, \phi)$ are orthonormal, no numerical integration over them is needed.

V. RESULTS

The vibrational energy levels for Ar₂-HF in $v = 0$ and 1, calculated using the complete nonadditive potential described above, are shown in Fig. 5. The levels shown are basically of two types. First, there are heavy-atom vibrations similar to those that exist in Ar₃ (or Ar₂-Ne) [32]. These can be thought of as built upon three normal modes: a symmetric (breathing) stretch (A_1 symmetry), an asymmetric stretch (A_1 symmetry), and an Ar₂ rock (B_2 symmetry). The asymmetric stretch and Ar₂ rock are degenerate for Ar₃, but not for Ar₂-HX. Secondly, there are vibrations due to hindered internal rotation of the HF molecule within the complex. The ground state correlates with HF ($j = 0$), while the next three HF bending levels correlate with HF ($j = 1$). The projection of j onto the intermolecular axis (or b axis) is approximately conserved, and is denoted k : the two $j = 1, |k| = 1$ states (Π states) are coupled by the ϕ dependence of the potential, and mix to form in-plane (B_2) and out-of-plane (B_1) bending states, while the $j = 1, k = 0$ state (Σ bend, A_1 symmetry) is unsplit and actually lies between the two Π states. This energy level pattern contrasts with that expected for the bending states of a near-rigid molecule, where the Σ bend is actually the *overtone* of the bending vibrations: in the present case, the Σ bend lies *below* the out-of-plane bend, so that it is clearly inappropriate to use the normal-mode description.

The main difference between the energy level diagrams for Ar₂-HF in $v = 0$ and 1 states is that, for $v = 1$, the excited HF internal rotor states move to higher energy



*Ground state. ^bIn-plane Π bend. ^c Σ bend. ^dOut-of-plane Π bend.

FIG. 5. Energy levels for Ar₂-HF ($v = 0$ and 1) calculated using the total nonadditive potential.

(relative to the ground state). This arises simply because of the increased anisotropy for $v = 1$. As a result, the levels correlating with HF $j = 1$ move upwards through the manifold of heavy-atom vibrational levels. The vibrational shift is most marked for the out-of-plane and Σ bending states. The Σ bend, in particular, moves from a reasonably isolated position for $v = 0$ into near degeneracy with an excited heavy-atom bending state for $v = 1$; the resulting states are strongly mixed in our calculations, with both mixed levels having a substantial amount of Σ bend character.

More details of our calculations are given in Table I for states of Ar₂-HF correlating with HF ($v = 0$ and 1) and in Table II for states correlating with HF ($v = 2$ and 3). The potentials listed are (i) the pairwise-additive potential formed from the Ar-Ar HFDID1 and Ar-HF H6(4,3,2) potentials; (ii) a potential including the anisotropic triple-dipole term of Eq. (4) as the only nonadditive contribution; (iii) the total nonadditive potential, including both the dispersion term and the new model of the induction and electrostatic distortion terms as described in Sec. II B; the three-body part of the total potential is shown in the bottom right panel of Fig. 4.

For $v = 0$, contour plots of the wave functions for the ground state, in-plane II bend, Σ bend, and the out-of-plane II bend are shown in Fig. 6. The ground state wave

function is concentrated around $\theta = 0^\circ$, and does not penetrate significantly beyond about $\theta = 80^\circ$. The in-plane and out-of-plane bends show very similar structure. Both peak at about $\theta = 50^\circ$ and spread considerably over the whole region in θ . The Σ bend wave function has maxima at both $\theta = 0^\circ$ and $\theta = 180^\circ$, with the larger peak corresponding to the H atom of HF pointing away from the Ar₂ midpoint.

The only experimental results so far available for Ar₂-HF in $v = 0$ are the rotational constants of the van der Waals ground state [11], which are measured as $A = 3576.5$ MHz, $B = 1739.1$ MHz, and $C = 1161.0$ MHz. The pairwise-additive calculations give results that differ from these by +26.5 MHz, +18.9 MHz, and +11.6 MHz. The triple-dipole term decreases the calculated rotational constants by between 2 and 7 MHz: it improves the agreement slightly, but not enormously. The total nonadditive potential, on the other hand, gives almost exact agreement with experiment for B and C , though A is still overestimated by 17.2 MHz.

The total nonadditive potential predicts reasonably intense far-infrared bending bands of Ar₂-HF with band origins around 60.0, 71.8, and 81.5 cm⁻¹. Measurements of these bands would provide very valuable information on the nonadditive forces.

For $v = 1$, the rotational constants of the van der

TABLE I. Results of the calculations for Ar₂-HF ($v = 0$ and 1).

Quantity	$v = 0$			$v = 1$		
	Additive	Dispersion	Total	Additive	Dispersion	Total
Ground state (A_1 symmetry)						
E_0 (cm ⁻¹)	-284.702	-281.937	-277.086	-300.056	-297.146	-291.663
Redshift (cm ⁻¹)				15.354	15.209	14.577
A (MHz)	3595.4	3588.9	3593.7	3593.8	3587.6	3593.6
B (MHz)	1765.6	1761.6	1739.2	1771.8	1767.3	1742.8
C (MHz)	1172.6	1170.0	1160.2	1175.5	1172.6	1162.1
Intensity	0.4974	0.4947	0.4645	0.5416	0.5389	0.5114
In-plane II bend (B_2 symmetry)						
ν_0 (cm ⁻¹)	64.044	63.655	60.046	66.348	65.907	62.000
A (MHz)	3619.3	3608.4	3641.3	3632.1	3622.1	3662.5
B (MHz)	1734.3	1730.7	1718.6	1735.1	1731.4	1715.7
C (MHz)	1158.0	1154.7	1154.8	1159.5	1156.2	1155.8
Intensity	0.1912	0.1889	0.2213	0.1760	0.1740	0.2076
Σ bend (A_1 symmetry)						
ν_0 (cm ⁻¹)	76.943	76.680	71.800	85.896	85.548	79.389 ^a
A (MHz)	3554.4	3537.9	3554.2	3579.2	3570.4	
B (MHz)	1744.0	1739.6	1743.8	1743.3	1738.0	
C (MHz)	1156.3	1152.1	1156.5	1157.9	1154.2	
Intensity	0.0617	0.0614	0.0761	0.0468	0.0475	0.058 ^b
Out-of-plane II bend (B_1 symmetry)						
ν_0 (cm ⁻¹)	85.223	84.901	81.495	91.703	91.320	87.575
A (MHz)	3550.5	3542.0	3540.5	3551.5	3543.0	3542.8
B (MHz)	1747.1	1743.1	1736.5	1749.0	1745.0	1736.8
C (MHz)	1158.2	1155.3	1152.2	1159.4	1156.5	1152.7
Intensity	0.1604	0.1609	0.1676	0.1451	0.1456	0.1514

^aStrongly mixed with a heavy-atom vibrational state; the other combination is at $\nu_0 = 80.498$ cm⁻¹.

^bIntensity summed over both mixed states with Σ bend character.

Waals ground state have been measured by McIlroy *et al.* [12] as $A = 3578.7$ MHz, $B = 1742.5$ MHz, and $C = 1163.0$ MHz. The comparisons with the three potentials are much the same as for $v = 0$: the pairwise-additive and dispersion-corrected potentials substantially overestimate all three rotational constants, while the total non-additive potential is in good agreement with experiment for B and C but overestimates A by 14.9 MHz. In addition, McIlroy *et al.* observed the shift between the band origin of Ar₂-HF and that of the HF monomer, which is a measure of the difference in binding energy between $v = 0$ and 1. The measured redshift is 14.827 cm⁻¹, which may be compared with the values of 15.354 and 14.577 cm⁻¹ calculated using the pairwise-additive and total nonadditive potentials, respectively.

Farrell and Nesbitt [17] have very recently observed the in-plane and out-of-plane HF bending combination bands of Ar₂-HF ($v = 1 \leftarrow 0$). For the out-of-plane band, their measured band origin is about 5.6 cm⁻¹ below the prediction of the pairwise-additive potential, but within 1.5 cm⁻¹ of the prediction of the total nonadditive potential. For the in-plane band, the measured band origin is 62.0 cm⁻¹, which is very close to the calculated result for the total nonadditive potential. Our previous

model of the exchange quadrupole gave an out-of-plane bending frequency about 81.4 cm⁻¹, overestimating the nonadditive shift by about 4.7 cm⁻¹, so that the model in the present paper is a clear improvement. The C rotational constant of the out-of-plane bend appears to be drastically overestimated by all the potentials. However, it is likely that this can be attributed to deficiencies in the computational method, and in particular to the neglect of Coriolis terms, rather than to the potential surfaces used.

Table I also gives calculations of the frequency of the Σ bend combination band. For the pairwise-additive and dispersion-corrected potentials, it is clear which calculated state corresponds to the Σ bend. However, for the total nonadditive potential for $v = 1$, there is strong mixing between the Σ bend and one of the heavy-atom vibrational states (see also Fig. 5), and both of the resulting levels have substantial calculated intensity. The heavy-atom vibrations are not as well converged as the HF internal rotations in our calculations, so it is difficult to make definite conclusions about the degree of mixing to be expected experimentally.

Table II gives predictions of the energy levels of Ar₂-HF for $v = 2$ and 3. The $v = 3$ levels are particularly

TABLE II. Results of the calculations for Ar₂-HF ($v = 2$ and 3).

Quantity	$v = 2$			$v = 3$		
	Additive	Dispersion	Total	Additive	Dispersion	Total
Ground state (A_1 symmetry)						
E (cm ⁻¹)	-317.095	-314.027	-307.917	-335.875	-332.638	-325.913
Redshift (cm ⁻¹)	32.393	32.090	30.831	51.173	50.701	48.827
A (MHz)	3590.9	3585.1	3592.3	3587.4	3581.6	3589.5
B (MHz)	1778.4	1773.9	1747.2	1785.8	1781.3	1752.7
C (MHz)	1178.4	1175.6	1164.2	1181.5	1178.7	1166.7
Intensity	0.5808	0.5782	0.5533	0.6156	0.6130	0.5903
In-plane Π bend (B_2 symmetry)						
ν_0 (cm ⁻¹)	69.046	68.553	64.366	72.082	71.540	67.089
A (MHz)	3644.2	3634.6	3682.5	3647.6	3634.6	3700.6
B (MHz)	1736.9	1732.7	1712.6	1740.1	1736.8	1710.2
C (MHz)	1161.3	1158.1	1156.6	1162.7	1159.2	1157.6
Intensity	0.1609	0.1589	0.1939	0.1426	0.1391	0.1805
Σ bend (A_1 symmetry)						
ν_0 (cm ⁻¹)	96.414	95.945	89.561	109.226 ^a	108.531 ^b	100.351
A (MHz)	3577.8	3573.4	3566.4			3566.6
B (MHz)	1739.1	1736.6	1729.1			1742.6
C (MHz)	1155.7	1154.4	1146.6			1154.4
Intensity	0.0326	0.0342	0.0372	0.022 ^c	0.024 ^c	0.0263
Out-of-plane Π bend (B_1 symmetry)						
ν_0 (cm ⁻¹)	99.066	98.621	94.614	107.051	106.549	102.373
A (MHz)	3550.8	3542.7	3543.4	3547.6	3540.2	3541.9
B (MHz)	1751.9	1747.6	1737.5	1756.0	1751.4	1739.2
C (MHz)	1160.9	1158.0	1153.4	1162.7	1159.7	11544.3
Intensity	0.1324	0.1329	0.1377	0.1222	0.1227	0.1267

^aStrongly mixed with a heavy-atom vibrational state; the other combination is at $\nu_0 = 108.654$ cm⁻¹.

^bStrongly mixed with a heavy-atom vibrational state; the other combination is at $\nu_0 = 107.784$ cm⁻¹.

^cIntensity summed over both mixed states with Σ bend character.

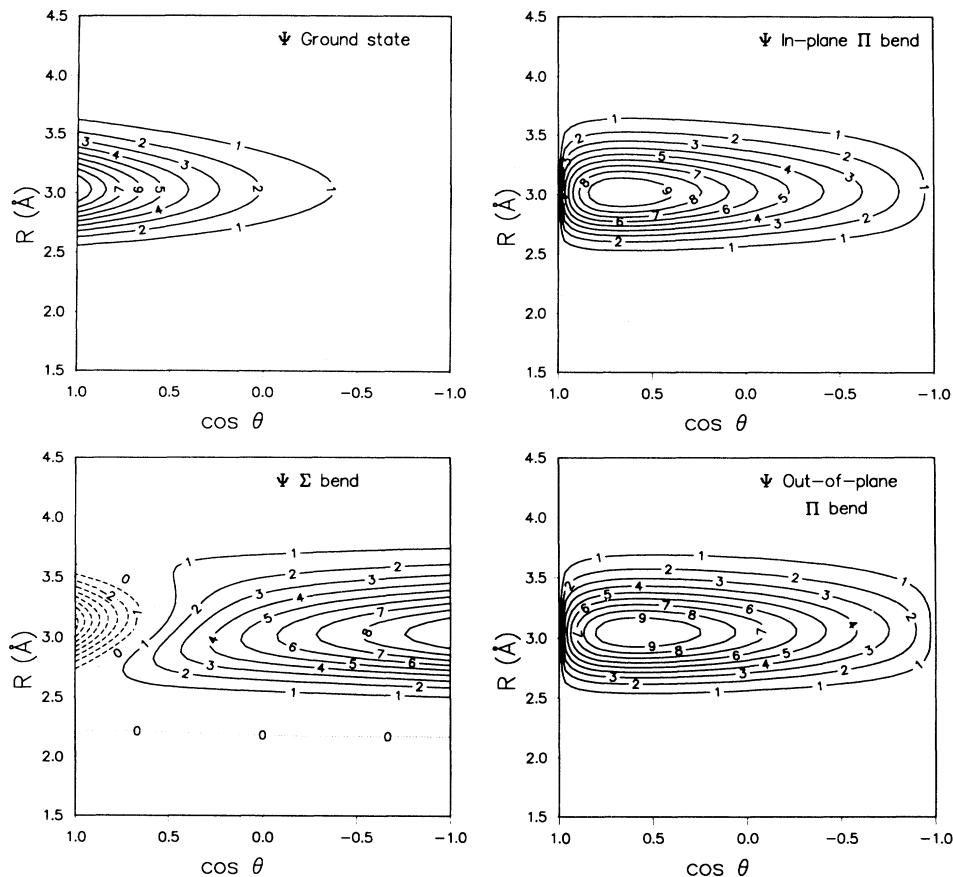


FIG. 6. Contour plots of wave functions for various states of $\text{Ar}_2\text{-HF}$ ($v = 0$), with $\rho = 3.757 \text{ \AA}$ and $R = 3.0 \text{ \AA}$: Ground state, with $\phi = 0^\circ$; in-plane Π bend, with $\phi = 0^\circ$; Σ bend, with $\phi = 0^\circ$; out-of-plane Π bend, with $\phi = 90^\circ$.

interesting, because second overtone spectra of van der Waals complexes such as Ar-HF can be measured with sensitivity comparable to that achieved in the HF fundamental region [43,22]. It would be very interesting to observe HF overtone spectra of $\text{Ar}_2\text{-HF}$, in order to extend our knowledge of the v dependence of nonadditive forces.

VI. CONCLUSIONS

We have carried out calculations on the $\text{Ar}_2\text{-HF}$ van der Waals trimer, using both pairwise-additive and non-additive interaction potentials. The calculations included all five low-frequency degrees of freedom, and also included a parametric dependence on the HF vibrational state. The results of the calculations are compared with experimental results from microwave and infrared spectroscopy.

As in earlier work on $\text{Ar}_2\text{-HCl}$, we have found substantial differences between the experiments and the calculations that use pairwise-additive potentials. In particular, the frequencies of HF bending (hindered internal rotation) bands have been observed up to 5 cm^{-1} lower than the pairwise-additive calculations. Less than 0.5 cm^{-1} of this discrepancy can be attributed to uncertainties in the Ar-HF and Ar-Ar pair potentials, and the remainder

must be due to nonadditive intermolecular forces.

We have investigated various ways of modeling the nonadditive intermolecular forces. Since the experiments deal with HF bending bands, the anisotropy of the non-additive terms is crucial. As for $\text{Ar}_2\text{-HCl}$, we have found that “conventional” types of nonadditive force, such as Axilrod-Teller triple-dipole forces and the interactions between induced dipole moments on the two Ar atoms, are much too weak to explain the observed effects. However, the shifts can be explained by invoking “exchange quadrupole” interactions, which arise from the interaction between the permanent multipole moments of the HF molecule and the quadrupole moment that develops on a pair of Ar atoms when their charge distributions overlap.

For $\text{Ar}_2\text{-HF}$, we found it necessary to use a more sophisticated model of the exchange quadrupole interaction than for $\text{Ar}_2\text{-HCl}$. Our earlier model, in which the Ar_2 charge distribution is represented by a single quadrupole located at the Ar_2 midpoint, drastically overestimates the nonadditive shifts for $\text{Ar}_2\text{-HF}$. Instead, we have used a distributed representation, in which the exchange quadrupole of Ar_2 is represented by equal and opposite dipoles located on the two Ar atoms. In addition, we have included a dispersion contribution to the Ar_2 quadrupole, and have also considered cross terms that arise due to interaction of the exchange dipoles on

the Ar atoms with the dipoles induced by the HF charge distribution. The resulting model gives a smaller total nonadditive energy, and gives reasonably good agreement with the observed infrared bending frequencies.

The present work has confirmed that, even for systems containing only one molecule, there are very important nonadditive interactions that do not arise in the purely atomic case. The dominant interaction in Ar₂-HF arises from the fact that the charge distributions of the constituents are modified by overlap effects, and this causes a substantial modification of the electrostatic interactions. Such effects may be expected to be important in all molecular systems, and will be very important in simulations of the properties of condensed phases.

ACKNOWLEDGMENTS

We are grateful to Adam Cooper for much early work on the computer programs, and to Lydia Heck, Richard Wheatley, and Keith Atkins for valuable discussions. We are also grateful to David Nesbitt and John Farrell for sending us their experimental results prior to publication. This work was supported by the European Commission. The calculations used a cluster of IBM RS/6000 computer work-stations belonging to the Atomic and Molecular Physics groups at Durham and Newcastle Universities, purchased under the SERC Computational Science Initiative. J.M.H. thanks the Nuffield Foundation for support.

-
- [1] R. J. LeRoy and J. M. Hutson, *J. Chem. Phys.* **86**, 837 (1987).
- [2] J. M. Hutson, *J. Chem. Phys.* **96**, 6752 (1992).
- [3] J. M. Hutson, *J. Phys. Chem.* **96**, 4237 (1992).
- [4] R. C. Cohen and R. J. Saykally, *J. Chem. Phys.* **98**, 6007 (1993).
- [5] C. A. Schmuttenmaer, R. C. Cohen, and R. J. Saykally, *J. Chem. Phys.* **101**, 146 (1994).
- [6] W. J. Meath and M. Koulis, *J. Mol. Struct.* **226**, 1 (1991).
- [7] T. D. Klots *et al.*, *J. Chem. Phys.* **86**, 5315 (1987).
- [8] M. J. Elrod, D. W. Steyert, and R. J. Saykally, *J. Chem. Phys.* **94**, 58 (1991).
- [9] M. J. Elrod, D. W. Steyert, and R. J. Saykally, *J. Chem. Phys.* **95**, 3182 (1991).
- [10] M. J. Elrod, J. G. Loeser, and R. J. Saykally, *J. Chem. Phys.* **98**, 5352 (1993).
- [11] H. S. Gutowsky *et al.*, *J. Chem. Phys.* **86**, 569 (1987).
- [12] A. McIlroy, R. Lascola, C. M. Lovejoy, and D. J. Nesbitt, *J. Chem. Phys.* **95**, 2636 (1991).
- [13] J. M. Hutson, J. A. Beswick, and N. Halberstadt, *J. Chem. Phys.* **90**, 1337 (1989).
- [14] A. R. Cooper and J. M. Hutson, *J. Chem. Phys.* **98**, 5337 (1993).
- [15] M. L. Elrod, R. J. Saykally, A. R. Cooper, and J. M. Hutson, *Mol. Phys.* **81**, 579 (1994).
- [16] A. Ernesti and J. M. Hutson, *Faraday Discuss. Chem. Soc.* (to be published).
- [17] J. T. Farrell and D. J. Nesbitt (unpublished).
- [18] G. Chałasinski, M. M. Szcześniak, and B. Kukawska-Tarnawska, *J. Chem. Phys.* **94**, 6677 (1991).
- [19] M. M. Szcześniak, G. Chałasinski, and P. Piecuch, *J. Chem. Phys.* **99**, 6732 (1993).
- [20] R. A. Aziz, *J. Chem. Phys.* **99**, 4518 (1993).
- [21] C. M. Lovejoy, J. M. Hutson, and D. J. Nesbitt, *J. Chem. Phys.* **97**, 8009 (1992).
- [22] H.-C. Chang *et al.*, *J. Chem. Phys.* **99**, 9337 (1993).
- [23] L. J. Rawluk *et al.*, *Chem. Phys. Lett.* **202**, 291 (1993).
- [24] S. Green and J. M. Hutson, *J. Chem. Phys.* **100**, 891 (1994).
- [25] A. S. Pine, *J. Chem. Phys.* **101**, 3444 (1994).
- [26] B. M. Axilrod and E. Teller, *J. Chem. Phys.* **11**, 299 (1943).
- [27] A. Kumar and W. J. Meath, *Mol. Phys.* **54**, 823 (1985).
- [28] D. E. Stogryn, *Phys. Rev. Lett.* **24**, 971 (1970).
- [29] E.-A. Reinsch and W. Meyer, *Phys. Rev. A* **14**, 915 (1976).
- [30] S. F. O'Shea and W. J. Meath, *Mol. Phys.* **28**, 1431 (1974).
- [31] S. F. O'Shea and W. J. Meath, *Mol. Phys.* **31**, 515 (1976).
- [32] A. R. Cooper, S. Jain, and J. M. Hutson, *J. Chem. Phys.* **98**, 2160 (1993).
- [33] L. Jansen, *Phys. Rev.* **125**, 1798 (1962).
- [34] A. R. Cooper, Ph.D. thesis, Durham University, 1992.
- [35] A. D. Buckingham, *Colloq. Int. CNRS* **77**, 57 (1959).
- [36] K. L. C. Hunt, *Chem. Phys. Lett.* **70**, 336 (1980).
- [37] G. Maroulis and D. M. Bishop, *J. Phys. B* **18**, 4675 (1985).
- [38] A. D. Buckingham, *Adv. Chem. Phys.* **12**, 107 (1967).
- [39] M. O. Bulanin, V. P. Bulychev, and K. G. Tokhadze, *J. Mol. Spectrosc.* **161**, 321 (1987).
- [40] I. P. Hamilton and J. C. Light, *J. Chem. Phys.* **84**, 306 (1986).
- [41] NAG FORTRAN Library, Mark 15, from Numerical Algorithms Group Ltd., Oxford, UK (1991).
- [42] A. Ernesti and J. M. Hutson, *Chem. Phys. Lett.* **222**, 257 (1994).
- [43] H.-C. Chang and W. Klemperer, *J. Chem. Phys.* **98**, 2497 (1993).